Article:
Fang, Hanlin, Liu, Jin, Li, Hongji et al. (6 more authors) (2018) 1305 nm Few-Layer MoTe2-on-Silicon Laser-Like Emission. Laser and Photonics Reviews. 1800015. ISSN: 1863-8899

https://doi.org/10.1002/lpor.201800015

Original Paper

1305 nm few-layer $MoTe_2$-on-silicon laser-like emission

Hanlin Fang[1,2†], Jin Liu[2†], Hongji Li[1,2], Lidan Zhou[1], Lin Liu[1], Juntao Li[1,2], Xuehua Wang[1,2], Thomas F. Krauss[3], Yue Wang[3]*

[†]These authors contributed equally to this work
[*]Corresponding Author: E-mail: lijt3@mail.sysu.edu.cn

[1]State Key Laboratory of Optoelectronic Materials and Technologies, Sun Yat-Sen University, Guangzhou, 510275, China
[2]School of Physics, Sun Yat-Sen University, Guangzhou, 510275, China
[3]Department of Physics, University of York, York, YO10 5DD, UK

Abstract: The missing piece in the jigsaw of silicon photonics is a light source that can be easily incorporated into the standard silicon fabrication process. Here, a silicon laser-like emission is reported that employs few-layer semiconducting transition metal dichalogenides of molybdenum ditelluride ($MoTe_2$) as a gain material in a silicon photonic crystal L3 nanocavity. An optically pumped $MoTe_2$-on-silicon lasing at 1305 nm, i.e. in the center of the "O-band" of optical communications, operating in the continuous-wave regime, is demonstrated at room temperature and with a threshold power density of 1.5 kW/cm^2. The surprising insight is that, contrary to common understanding, a monolayer $MoTe_2$ is not required to achieve higher efficiency laser-like emission operation. Instead, few-layer $MoTe_2$ offers a higher overlap between the two dimensional (2D) gain material and the optical mode for sufficient gain. The ability to use few-layer material opens new opportunities for deploying manufacturing methods such as chemical vapor deposition and thereby brings 2D-on-silicon devices a step closer to becoming a scalable technology.

1. Introduction

Due to its excellent integratability and compatibility with CMOS technology, silicon photonics has been widely recognized as the most promising platform for a future broadband, high-speed data transmission infrastructure. [1] Photonics offers substantial reductions in operating energy and improvements in the performance of data communication systems, which explains its wide use in datacentres. [2] While many essential silicon photonics components have already been demonstrated with excellent performance, such as extremely low-loss waveguides, [3] ultra-fast modulators, [4] and high bandwidth detectors, [5] a silicon light source, e.g. a silicon laser, which can be easily incorporated into the standard fabrication process, has remained a challenge.

Silicon itself is a poor light emitter due to its indirect bandgap, so a combination with suitable light emitting materials is necessary. Most notably, the hybrid integration of III-V materials with silicon has made significant progress, [6, 7] but the approach is costly and complex, so there is still an appetite for exploring alternative solutions. Optical frequency combs (OFCs) [8, 9] is another way for silicon emission source, however, it cannot be electrically pumped and needs high pump power, which make it difficult to integrate into an optical interconnect. The molybdenum ditellurite ($MoTe_2$)-on-silicon laser we present here is such a promising alternative, especially as it operates in the centre of the technologically important 1260 - 1360 nm wavelength range, also known as the “O band” in fibre-optic communications.

$MoTe_2$ is one of a family of two-dimensional (2D) materials that were spawned out of the graphene revolution. Many of these 2D materials, especially atomically thin transition metal dichalcogenides (TMDs) such as tungsten diselenide (WSe_2), molybdenum disulfide (MoS_2) and now $MoTe_2$, exhibit remarkable optoelectronic properties, such as strong exciton binding energy and high carrier mobility. [10-14] 2D materials are special as their atoms are

strongly bonded in the plane but only weakly attached out-of-plane; this weak interaction between layers makes the extraction of a single or a few-layer sheet of atoms possible, which underpins this burgeoning research area. [15] Excitingly, several TMD-based lasers have now been demonstrated, including a continuous-wave (CW) WSe_2 monolayer laser emitting around 740 nm at 80 K, based on a gallium phosphide photonic crystal (PhC) cavity, [16] a microdisk laser including a tungsten disulfide (WS_2) monolayer that is sandwiched by a Si_3N_4 and hydrogen silsesquioxane (HSQ), operating at 612 nm and at 10 K, [17] and a room temperature four layer MoS_2 laser emitting in the wavelength range of 600 to 800 nm, based on a vertically coupled microdisk and microsphere cavity. [18] Whereas these initial demonstrations were focussed on the visible regime, a TMD-based laser operating in the silicon transparency window at 1132 nm has been demonstrated very recently, [19] using a silicon nanobeam cavity and a monolayer of $MoTe_2$ as the gain material. Our work now demonstrates that the operating wavelength can be pushed further into the infrared and into the 1260 nm to 1360 nm communications window ("O band"), which signifies a technological step-change for this type of laser.

Secondly, in order to achieve low threshold operation, we investigate the impact of two significant factors: the quality (Q)-factor of the nanocavity and the optical mode confinement factor Γ. These two factors are brought together in the laser threshold condition, which can be described in terms of Q and Γ as follows:

$$\frac{2\pi n_{eff}}{\lambda}\frac{1}{Q} = \Gamma g_{th} \qquad (1)$$

where the left-hand side contains the loss in terms of Q-factor, Q, while the right-hand side contains the threshold gain, g_{th}. From Equation (1), it is obvious that low-threshold operation can be achieved if both the cavity Q-factor and the Γ-factor are high. Microscopically, a high Q-factor will help the atomically thin material to provide sufficient optical gain to reach the

laser threshold. As the 2D gain material sits on top of the nanocavity and not at the centre of the waveguide, it is equally important to consider the mode overlap factor Γ in order to reduce the laser threshold.

Next, let us consider the advantages of using few-layer $MoTe_2$ as the gain medium instead of monolayers for laser operating at 1300 nm. At 1300 nm, the photoluminescence (PL) efficiency, as well as the gain, of $MoTe_2$ monolayers is very similar to that of few-layer sheets. [20,21] Therefore, using few-layer $MoTe_2$ as the gain medium for 1300 nm emission can benefit from multiple aspects: (1) high-quality, few-layer $MoTe_2$ can now be grown by chemical vapor deposition (CVD) [22] in a relatively large size (> 2 cm^2), while monolayers obtained either by CVD growth [23] or by mechanical exfoliation [19] are currently limited to sizes of 100s of μm^2; (2) similarly, the fabrication tolerances increase when stringent layer control is not required, (3) the gain peak red-shifts with increasing layer thickness [20,21] and (4) the mode overlap Γ is significantly larger when employing few-layer material. [18] We believe that the latter point is pivotal to achieving the low-threshold operation we report here.

2. Photoluminescence from atomically thin $MoTe_2$ flakes

The layer-dependent PL of $MoTe_2$ has already been reported both at cryogenic and at room temperature on a range of substrates. [20, 24] At low temperature, the PL emission spectrum consists of a split peak, of which the high and low energy points represent the exciton and trion emission, respectively. With an increase in temperature, the energy of the trions transfers to the excitons, resulting in a redshift of the emission. In contrast to other TMDs, the PL quantum yield of $MoTe_2$ remains relatively high from mono- up to few-layers. [20]

The $MoTe_2$ layers studied here were exfoliated from bulk material (obtained from HQ graphene, The Netherlands) and then transferred onto the silicon substrate by means of an all-dry transfer technique. [25] Figure 1 shows the PL emission from bi-, tri- and penta (5)-layer $MoTe_2$ flakes on a silicon substrate at room temperature, with the emission peak wavelength

shifting from 1130 nm to 1170 nm. Concurrently, the PL emission intensity at 1305 nm increases slightly between 2- and 5-layer $MoTe_2$. The mode overlap factor Γ commensurately increases with layer thickness (see Supporting Information (SI) for a detailed calculation).

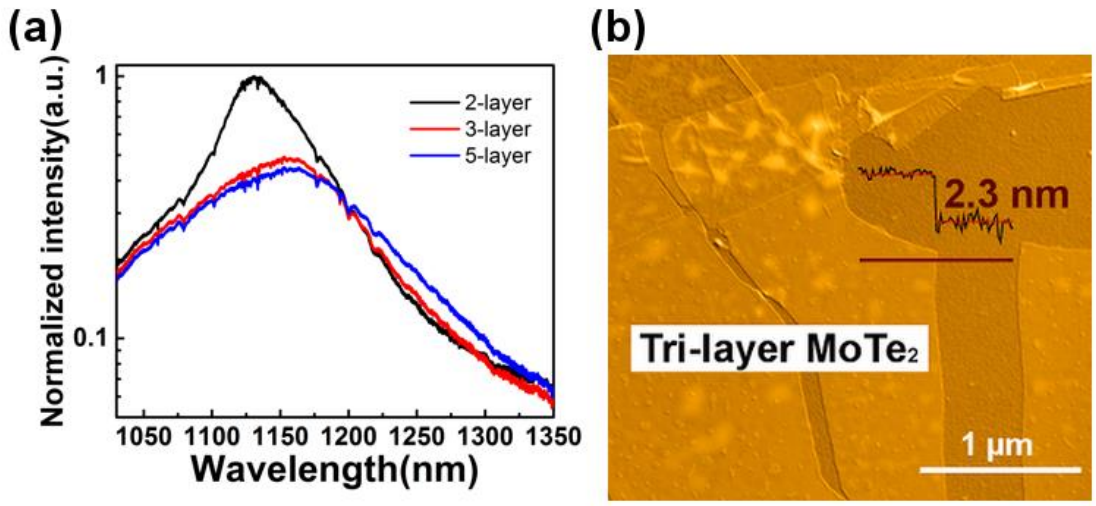

Figure 1. PL characterization. PL emission obtained at room temperature of bi-, tri- and penta (5)-layer $MoTe_2$ flakes. (**a**) PL spectra collected with a 785 nm CW excitation laser (1.68 mW excitation power and 1 μm spot size on the sample surface). (**b**) Corresponding atomic force microscope (AFM) profile showing the thickness of the tri-layer $MoTe_2$ flake exfoliated on a silicon substrate. Since a monolayer is approximately 0.7 nm thick, 2.3 nm represents a trilayer.

3. Nanocavity for $MoTe_2$-on-silicon laser-like emission

At the wavelength of 1130 nm, the intrinsic absorption loss in silicon is approximately 6.5 dB/cm. Although this loss is sufficiently low to enable the demonstration of high quality (Q-factor) photonic crystal (PhC) cavities, [19] the practical telecommunication wavelength range starts at 1260 nm, where the loss in silicon drops to well below 0.01 dB/cm. Regarding the $MoTe_2$ gain material, we observe a similarly favourable trend with moving to longer wavelength, as the absorption coefficient of $MoTe_2$ drops from 2.4 x 105 cm^{-1} at 1130 nm to 6

x 103 cm^{-1} at 1300 nm. [26] Hence an operating wavelength of 1300 nm is possible even though the PL emission of $MoTe_2$ at that wavelength appears low (Figure 1a). Realising these advantages in addition to the benefits of few-layer material operation outlined above, we targeted a wavelength of 1300 nm and fabricated a number of PhC nanocavities in this range, using silicon-on-insulator (SOI, Soitec) material with a nominal 220 nm thick device layer on 2 µm of buried oxide.

The nanocavities are of the L3 geometry, which consists of a line defect of 3 missing holes in a triangular lattice. [27] Additionally, we implemented the far-field optimisation method in order to increase the out-of-plane coupling of the cavity mode. [28] An example of such a far-field optimised PhC cavity with its corresponding radiation pattern is illustrated in Figure 2 (a-b). Following fabrication (see Methods) we measured a Q-factor of Q = 5900 for such a cavity in its "unloaded" condition, i.e. before applying the $MoTe_2$ flake onto it, at a resonant wavelength of 1298 nm (see Figure S3). We calculate a coupling efficiency of 80% for this cavity using an objective with N.A. = 0.65 for the measurement (Figure S2). This high coupling efficiency is essential for coupling the laser emission to free space, and thus making the observation of laser operation possible.

The $MoTe_2$ flakes are precisely placed on top of the cavity, as shown in the optical micrograph and on the SEM micrographs (see Figure 2 (c-d)). The AFM profile indicates that the $MoTe_2$ flake on the centre of the L3 cavity is 3.7 nm thick, i.e. consisting of approximately 5 layer. It is worth noting that the thickness of the $MoTe_2$ flake is not uniform over the whole cavity. As shown in the following section, this non-uniformity does not influence lasing performance, as the PL emission at 1300 nm is relatively insensitive to layer number (Figure 1a), which also highlights the fabrication tolerances of our device.

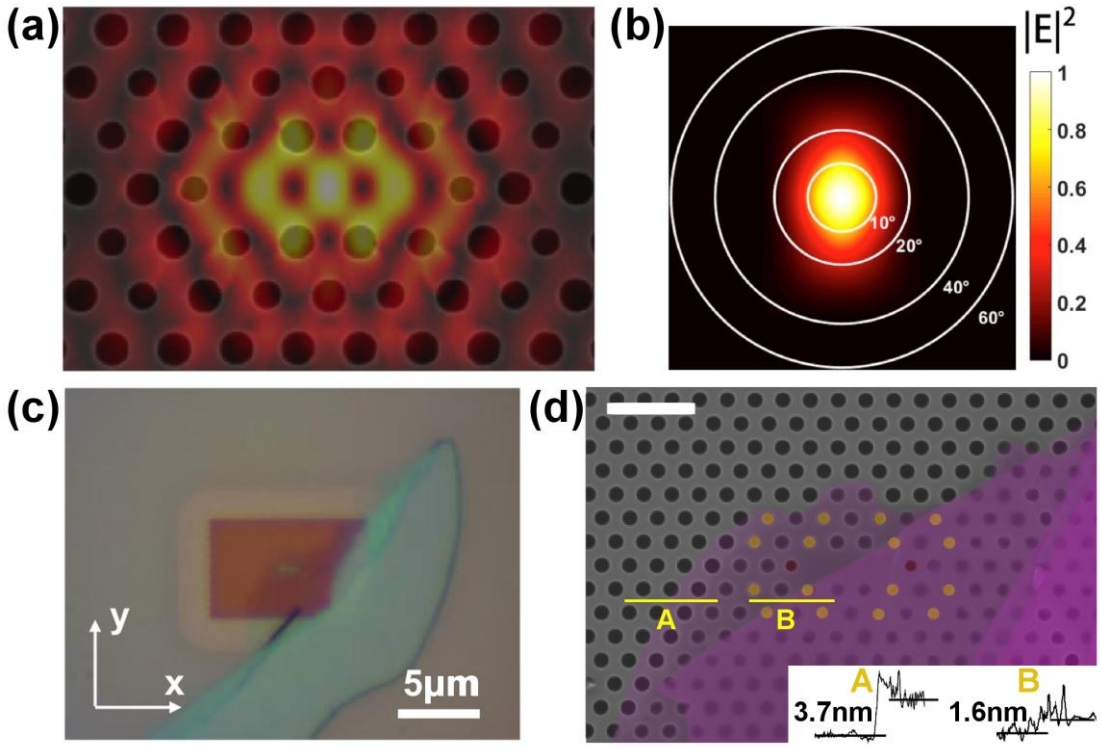

Figure 2. $MoTe_2$ on silicon photonic crystal cavity. Calculated electric field profile $|E|^2$ of a L3 PhC nanocavity for (**a**) the fundamental mode M1 and (**b**) its corresponding far-field emission. (**c**) Optical micrograph and (**d**) false-colored SEM image of a few-layer $MoTe_2$ flake on the silicon PhC cavity and corresponding AFM topography profiles; the scale bar in (d) represents 1 μm. We define the x and y directions in (c) to align with the ΓK and ΓM direction of the PhC cavity, respectively.

4. Dual-mode $MoTe_2$-on-silicon laser-like emission at room temperature

We pump the sample with a 785 nm CW laser at room temperature and observe laser-like emission at 1305 nm (Mode M1 in Figure 3). There is a second peak at 1250 nm (Mode M2), which we assign to a higher order resonance of the cavity. Here, the excitation power is measured after the objective, i.e. directly on the sample. In order to determine the emission power, we use an external 1340 nm CW laser as a calibration source and first measure the total loss of the optical elements between the sample and the spectrometer, then calculate the actual emission power based on the photon counting number registered by the detector. The

excitation power on the cavity for the measurement of Figure 3 is 1.9 mW, i.e. well above threshold. The emission spectra were collected with a 50x objective (N.A. = 0.65) as a function of the pump intensity. We note that the emission is strongly polarised perpendicular to the direction of the line defect, corresponding to laser oscillation along the defect as expected for this cavity geometry (inset of Figure 3).

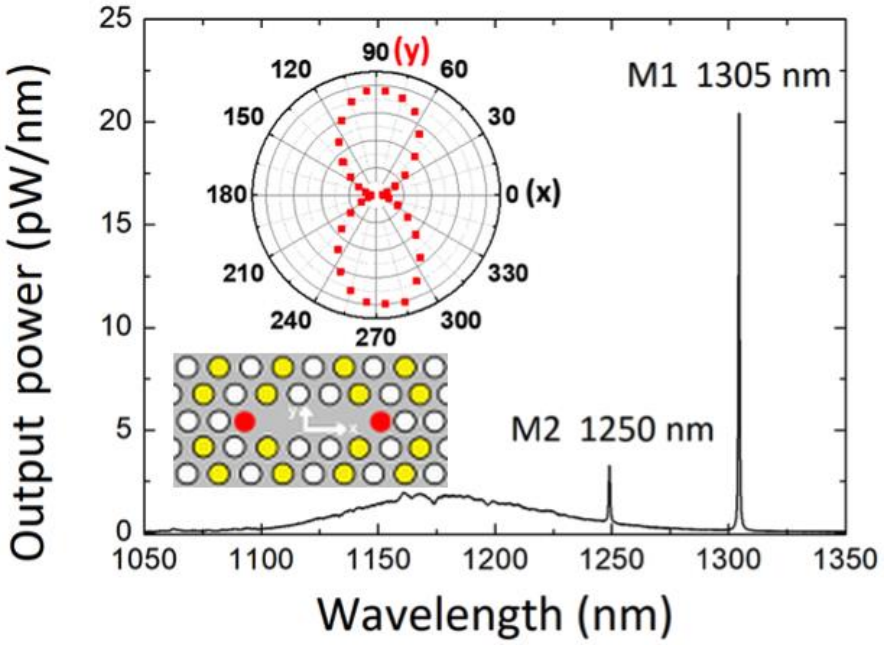

Figure 3. Dual-mode emission and polarisation. Emission spectrum of optically pumped $MoTe_2$-on-silicon laser-like emission at room temperature with a pump power of 1.9 mW; the fundamental mode (M1) is observed at 1305 nm and a higher order mode (M2) at 1250 nm. Inset: polarization characteristic of the M1 mode, with the x and y directions indicating the L3 cavity orientation, using the same coordinate system as in Figure 2.

It is interesting to note that the emission power of the M1 mode is much higher than that of the M2 mode, even though the PL efficiency at the wavelength of the M1 mode is lower than that of the M2 mode and their Q values are similar. This behaviour is explained by the far-field emission pattern, which is optimised for the M1 mode but not for M2. The

corresponding output power density, i.e. the integrated power of the fundamental cavity mode M1 as a function of input pump power density, is plotted in Figure 4a, showing the familiar nonlinear 'kink' around threshold. Here, the input power density uses the measured pump spot diameter of 1.72 μm (see Figure S4) and the output power density takes into account the active area of the PhC cavity of 1.25 μm^2. The kink is not particularly pronounced due to the high spontaneous coupling, β coefficient, which is discussed in more detail below. The spontaneous emission power from an "off-resonant" position at the same wavelength, which does not show lasing, is also plotted in Figure 4a for comparison. This off-resonant power is much smaller than the on-resonant power because of a combination of extraction efficiency and Purcell-factor. [29] At low pump intensity, we observe an emission peak with a linewidth of 0.520 nm (full width at half maximum, FWHM), as shown in Figure 4 (b-c). Once the pump power is increased above 1.75 kW/cm^2, the peak narrows down to below 0.495 nm. When increasing the pump power above threshold, linewidth re-broadening is observed, which we explain with an increase in carrier-density and corresponding loss with pump power. [19]. Notice that the linewidth change is not as obvious as expected. We believe that this larger linewidth is due to some, yet unexplained, self-pulsation effect. For example, it is known that TMDs are good saturable absorbers and that they can be used to generate both Q-switched and passively mode-locked lasing. [30, 31] Hence, we believe that our $MoTe_2$ laser-like device operates in a self-pulsation mode, [32] which is responsible for the linewidth being broader than expected for a cw laser above threshold. Figure 4c shows the Lorentzian fits to the fundamental mode emission spectra taken at different pump powers (see Figure S6 for more details). The "hot cavity" Q-factor calculated from these fits is $Q \approx 2{,}660$.

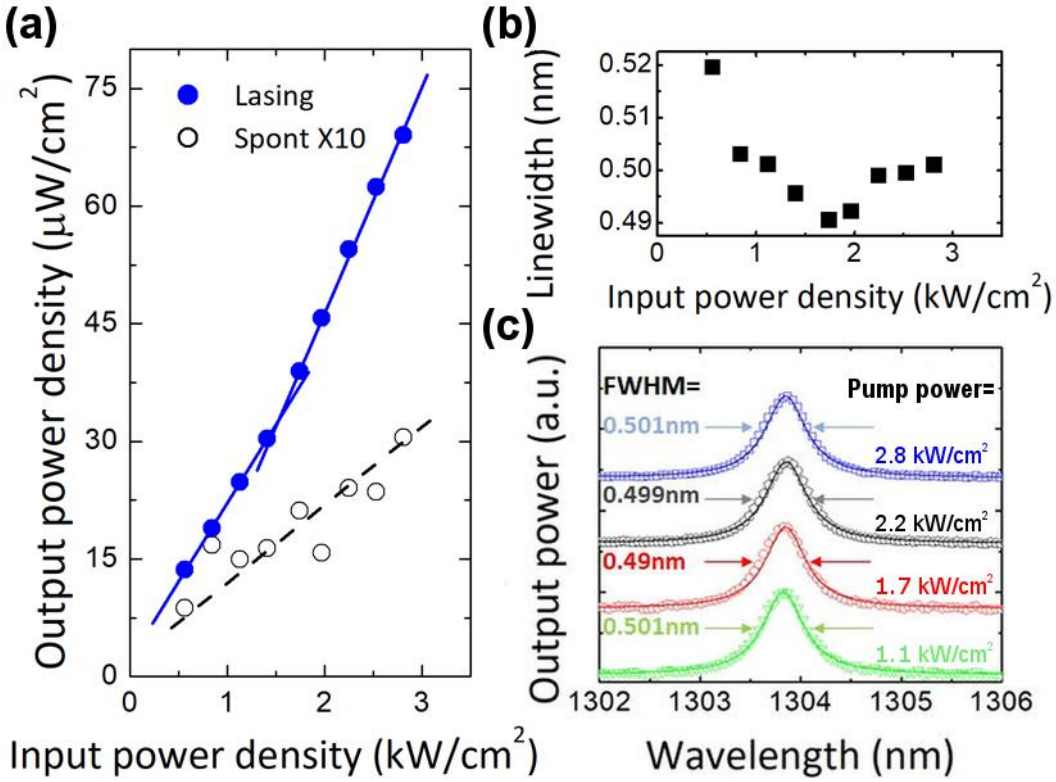

Figure 4. Laser threshold and linewidth. (**a**) The output power density of the fundamental laser mode (blue dots) and spontaneous emission (magnified by 10) at the same wavelength (black circles) as a function of pump power density incident on the sample surface. The fitted straight lines are guides to the eye. The kink in the laser emission indicates a lasing threshold of 1.5 kW/cm^2. (**b**) Linewidth of emission at 1305 nm as a function of the pump power. (**c**) Fundamental mode output spectra (dots) and the corresponding Lorentzian fits (solid curves) for different pump powers.

5. Examining few-layer $MoTe_2$ laser-like emission performance

As shown in Figure 3, we determine the $MoTe_2$ laser-like emission power density to be approximately 1.6 mW/cm^2 (20 pW) with a pump power of 1.9 mW. Although this output power is weaker than that of other compact silicon lasers, [33, 34] we believe that our work represents the beginning of a new area, because there is considerable scope for improvement. For example, one could incorporate the $MoTe_2$ gain material directly into the waveguide

material, thereby increasing the overlap factor further, or construct a distributed coupled-cavity array-type laser [35] which would be able to draw on a larger gain volume, thus enabling potential applications in optical communications and interconnects.

To further verify laser operation, we fit our experimental data to the laser rate equation (for more detail see SI) and determine a lasing threshold of 1.5 kW/cm^2 (35 μW) for the M1 mode. Meanwhile, the β-factor, defined as the fraction of spontaneous emission coupled into the cavity mode, is obtained to be 0.5 for M1 mode and 0.48 for M2 mode. These β-factors are similar to others reported in the literature [17, 18] and result from the strong cavity–gain coupling in the planar $MoTe_2$-on-silicon geometry. We note that these values represent an "apparent" β-factor, however, which are enhanced by the Purcell factor, so the real beta factor is lower (see "Laser rate equation analysis" in the SI for more detail).

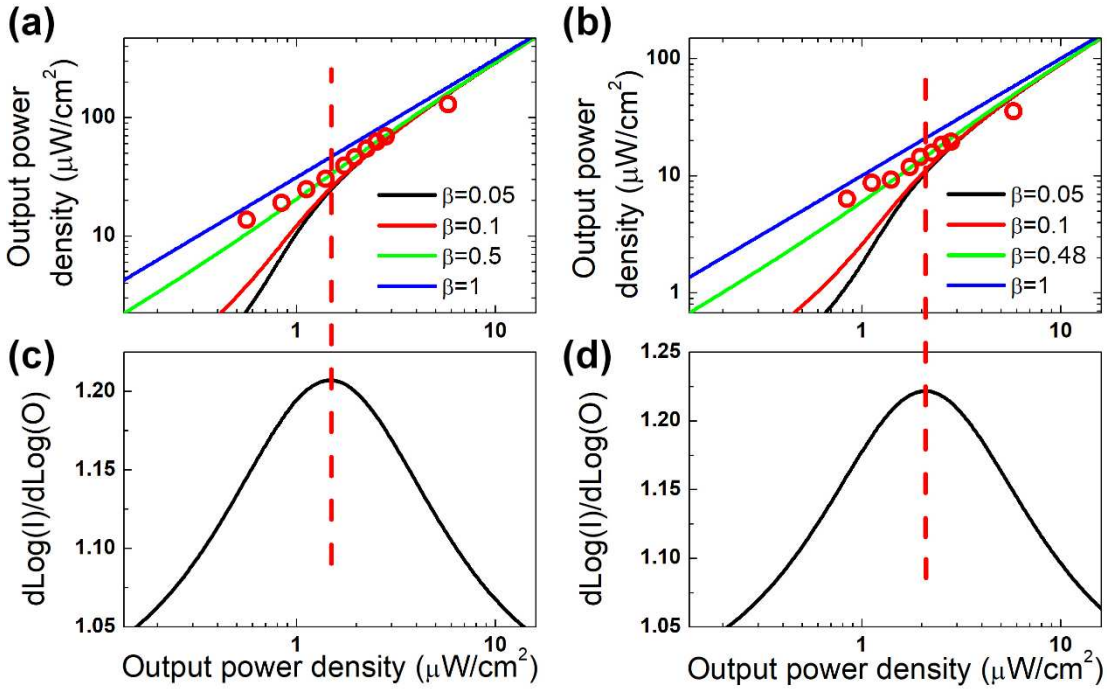

Figure 5. Laser threshold and β-factor. (**a**-**b**) Output power density as a function of the excitation power density of (**a**) the M1 and (**b**) the M2 mode. The red dots represent experimental data and the solid curve is a fit to the laser rate equation, corresponding to a

spontaneous emission coupling factor $\beta = 0.5$ for M1 and $\beta = 0.48$ for M2. Calculated curves for other values of β are plotted for comparison. (**c**-**d**) First order derivative curve of the laser rate equation of M1 and M2 mode respectively - the vertical dashed lines (red) indicate the peak position, i.e. lasing thresholds (see SI).

Finally, by simply changing the periods of the PhC cavity, we are able to achieve a wide tuning range of the lasing wavelength. The laser emission peak can be tuned from 1127 nm to 1305 nm by varying the period of the PhCs between 272 nm and 328 nm (see Figure S5).

6. Discussion

It is interesting to compare our results to those already published, so to better understand the impact of the nature of the TMDC and the properties of the PhC cavity, see Table 1.

Table 1. Performance comparison of various 2D material based lasers

Reference	Gain Material	Lasing Wavelength (nm)	Operating Temperature (K)	Pump Source	Hot cavity Q-factor[a)]	Threshold[b)] (W/cm^2)
[16]	WSe_2	740	130	CW	2,465	1
[17]	WS_2	612	10	Pulse	2,605	5-8 x 10^6
[18]	MoS_2	600-800	300	CW	~3,000	7140
[19]	$MoTe_2$	1132	300	CW	5,603	2100 [2c)]
This work	$MoTe_2$	1305	300	CW	2,660	1500

[a)]The "hot cavity" Q factor is derived from the lasing mode; [b)]We calculate the threshold from the total power incident on the sample surface and divide it by the pump spot area without taking any other effects such as power coupling into account; [c)]The threshold value in [19] is

reported to be 6.6 W/cm^2. This quoted value is lower because the authors took absorption and coupling coefficients into account, which is not typically done by other authors.

In Table 1, we determined the threshold from the power incident on the device and the spot size as is typically done, and without taking any correction factors into account. This may lead to deviations between the values shown here and those published, e.g. for [19], but it gives a better comparison and provides more insight.

As shown in Table 1, we achieve the lowest threshold lasing at room temperature from 2D materials, even though our Q-factor is not the highest. We believe that this improved performance can be attributed to two effects: (1) the optical gain of $MoTe_2$ at 1300 nm remains high even for few-layer; commensurately, the overlap between the gain material and the optical mode increases with layer thickness (see SI for further discussion); (2) $MoTe_2$ exhibits high gain even at room temperature, and is one of the best candidates so far for active materials emitting in the near-infrared.

Considering the recent demonstrations of $MoTe_2$-based silicon photonic devices including an 1132 nm optically pumped laser [19] and a 1175 nm electrically pumped light-emitting diode, [36] we believe that our laser-like emission operating at 1305 nm, i.e. in the centre of the communications “O-band”, offer a real promise for an integrated low-cost electrically pumped nanoscale silicon light source, thereby adding an essential building block to the silicon photonics platform.

7. Conclusions

In summary, we have demonstrated a room-temperature laser-like emission based on atomically thin semiconducting material in the optical communication band. By employing $MoTe_2$ as the gain material, which has maximum PL efficiency at around 1150 nm (1.08 eV) at room temperature, it was surprising that we can achieve lasing at 1305 nm (0.95 eV) by

optimising the silicon cavity structure and using few-layer $MoTe_2$. This demonstration thus not only contributes to the establishment of 2D TMDs as practical novel gain media but also has remarkable impact on silicon photonics where on-chip silicon light sources are highly desired. With an excitation threshold as low as 1.5 kW/cm^2 and a reasonable emission power, our demonstration of 2D-on-silicon nanolasers could lead to exciting applications in on-chip optical communications and interconnects. Furthermore, our demonstration of lasing in few-layer $MoTe_2$ heralds that manufacturing tolerance can be increased, and low cost commercial devices can be achieved by CMOS processing and large-scale CVD growing of $MoTe_2$. We can also foresee that with further optimisation of the cavity, e.g. fine adjustment of the PhC to achieve higher Q values and by employing larger cavity geometries, the threshold can be further reduced and the laser output power can be further increased. On the other hand, we would put more attentions to the optical properties of 2D materials itself with the focus of maximizing the PL gain, e.g., chemical treatment, [37] engineering the band-structure in van der Waals heterostructures. [38]

8. Methods

8.1. Design and characterization of the PhCs cavity

To provide the cavity feedback, we used a far-field optimised L3-type planar PhC cavity structure (see Figure S1). We performed 3D FDTD simulations to obtain the desired cavity modes. First, we fixed the value of *r/a*, i.e. the ratio of the hole radius (*r*) and the period (*a*), then changed r and a, respectively to obtain the resonant wavelength of the PhC cavities to be around 1300 nm. Secondly, the Q-factor and the far-field were optimized by changing the hole size (r) and hole positions around the L3 cavity. The optimized parameters of the final design are detailed in Table S1. This design achieved an excellent compromise between the Q-factor and the far-field emission pattern for the M1 mode. The Q-factor of the PhC cavity is

measured by detecting the cross-polarised resonantly scattered light from a normally incident white light source (see Figure S3).

8.2. Fabrication of the PhC cavities

The PhC cavities were fabricated on a SOITEC SOI wafer comprising a 220 nm thick silicon layer on a 2 μm sacrificial silicon dioxide layer. The pattern was defined in ZEP520A electron beam resist by electron-beam lithography (Raith Vistec EBPG5000+ 100kV), and then transferred into the silicon membrane using an inductively coupled plasma system (Oxford PlasmaPro 100ICP180) with HBr gas. The residual resist was removed by a microresist remover 1165. The silica beneath the PhC cavity was finally removed with the sample submerged in a hydrofluoric acid bath.

8.3. Exfoliation and transferring the 2D flakes

To prepare the 2D materials, the $MoTe_2$ flakes were initially exfoliated onto a PDMS stamp. Their thicknesses were confirmed using an optical microscope and an AFM (Bruker BioScope Resolve). After preparing the 2D material, we used the dry transfer technique [25] to transfer the few-layer $MoTe_2$ onto the silicon PhC cavity.

8.4. Laser performance characterisation

Pump power density is an important parameter of any laser performance. Therefore, we need to measure the size of the pump beam precisely. Firstly, we used a gold marker of 10 μm size to calibrate our microscope imaging system with an electron multiplying charge-coupled device (EMCCD: Andor DU-888U3-CS0-BVF), noting that the size of each pixel projected onto the image is 0.187 μm. Then the pump spot on the silicon sample surface was captured by the EMCCD camera. The spot intensity data was acquired by the grey value profile and then fitted with a Gaussian curve to obtain the FWHM. The FWHM of the pump beam in our laser measurements was measured to be 1.72 um, as shown in Figure S4. To optically excite

the $MoTe_2$-on-silicon laser, a 785 nm CW laser was focused through a 50x objective (NA = 0.65) onto the active gain material. The spectra were collected by an IR spectrometer with a 600 line/mm grating (Princeton Instrument SP2758), which corresponds to a spectral resolution of 0.2 nm, and a nitrogen cooled CCD (Princeton Instrument OMA-V:1024/LN).

Supporting Information

Figure S1: Schematic of far-field optimized PhC cavity of the L3-type.

Figure S2: Calculation of extraction efficiency.

Figure S3: Cavity Q-factor measurement.

Figure S4: Excitation laser spot size measurement.

Figure S5: Tunability of the few-layer $MoTe_2$-on-silicon laser-like emission

Figure S6: Power dependence of lasing-like action

Table S1: Design parameters of the PhC cavity

Table S2: Definitions and values of parameters used in the rate equations

Acknowledgements. This work is supported by National Key R&D Program of China (2016YFA0301300), National Natural Science Foundation of China (11674402, 11334015), Guangzhou Science and Technology projects (201607010044, 201607020023), Natural Science Foundation of Guangdong (2016A030312012), the Fundamental Research Funds for the Central Universities, and the EPSRC of the UK, Grant EP/M015165/1 (Ultrafast Laser Plasma Implantation- Seamless Integration of Functional Materials for Advanced Photonics). We would also like to acknowledge Prof. Xuetao Gan at Northwestern Polytechnical University, China for useful discussion on exfoliating and transferring 2D materials.

Keywords: Few-layer, molybdenum ditelluride, photonic crystal cavity, silicon laser, O-band.

Author contributions: J.Li and Y.W. conceived the work, designed the research strategy and directed the project. H.F., J.Liu, L.Z., L.L. and Y.W. fabricated the silicon nanocavities. H.F., J.Liu, H.L. and X.W. developed the FDTD simulations and laser equation fittings. H.F. and H.L. fabricated the $MoTe_2$-on-silicon samples. H.F., H.L. and J.Li performed the PL and laser measurements. Y.W. performed the AFM measurements. H.F., J.Li, T.F.K. and Y.W. analysed the data and wrote the manuscript. All the authors participated in the discussions and manuscript revisions.

References

[1] A. E.-J. Lim, S. Junfeng, F. Qing, L. Chao, T. Xiaoguang, D. Ning, C. Kok Kiong, R. P.-C. Tern, L. Tsung-Yang, *Quantum Electron.* **20**, 405-416 (2014).

[2] D. Dai, J. Bauters, J. E. Bowers, *Light Sci. Appl.* **1**, e1 (2012).

[3] M. J. R. Heck, J. F. Bauters, M. L. Davenport, D. T. Spencer, J. E. Bowers, *Laser Photon. Rev.* **8**, 667-686 (2014).

[4] G. T. Reed, G. Mashanovich, F. Y. Gardes, D. J. Thomson, *Nat. Photon.* **4**, 518-526 (2010).

[5] J. J. Ackert, D. J. Thomson, L. Shen, A. C. Peacock, P. E. Jessop, G. T. Reed, G. Z. Mashanovich, A. P. Knights, *Nat. Photon.* **9**, 393-396 (2015).

[6] D. Liang, J. E. Bowers, *Nat. Photon.* **4**, 511-517 (2010).

[7] Z. Zhou, B. Yin, J. Michel, *Light Sci. Appl.* **4**, e358 (2015).

[8] P. Del'Haye, A. Schliesser, O. Arcizet, T. Wilken, R. Holzwarth, T. J. Kippenberg, *Nature* **450**, 1214-1217 (2007).

[9] A. Dutt, C. Joshi, X. Ji, J. Cardenas, Y. Okawachi, K. Luke, A. L. Gaeta, M. Lipson, *Sci. Adv.* **4**, e1701858 (2018).

[10] K. F. Mak, C. Lee, J. Hone, J. Shan, T. F. Heinz, *Phys. Rev. Lett.* **105**, 136805 (2010).

[11] Q. H. Wang, K. Kalantar-Zadeh, A. Kis, J. N. Coleman, M. S. Strano, *Nat. Nanotechnol.* **7**, 699-712 (2012).

[12] F. Xia, H. Wang, D. Xiao, M. Dubey, A. Ramasubramaniam, *Nat. Photon.* **8**, 899-907 (2014).

[13] G. R. Bhimanapati, Z. Lin, V. Meunier, Y. Jung, J. Cha, S. Das, D. Xiao, Y. Son, M. S. Strano, V. R. Cooper, L. Liang, S. G. Louie, E. Ringe, W. Zhou, S. S. Kim, R. R. Naik, B. G. Sumpter, H. Terrones, F. Xia, Y. Wang, J. Zhu, D. Akinwande, N. Alem,

J. A. Schuller, R. E. Schaak, M. Terrones, J. A. Robinson, *ACS Nano* **9**, 11509-11539 (2015).

[14] A. Bablich, S. Kataria, M. Lemme, *Electronics* **5**, 13 (2016).

[15] K. S. Novoselov, A. Mishchenko, A. Carvalho, A. H. Castro Neto, *Science* **353**, aac9439 (2016).

[16] S. Wu, S. Buckley, J. R. Schaibley, L. Feng, J. Yan, D. G. Mandrus, F. Hatami, W. Yao, J. Vuckovic, A. Majumdar, X. Xu, *Nature* **520**, 69-72 (2015).

[17] Y. Ye, Z. J. Wong, X. Lu, X. Ni, H. Zhu, X. Chen, Y. Wang, X. Zhang, *Nat. Photon.* **9**, 733-737 (2015).

[18] O. Salehzadeh, M. Djavid, N. H. Tran, I. Shih, Z. Mi, *Nano Lett.* **15**, 5302-5306 (2015).

[19] Y. Li, J. Zhang, D. Huang, H. Sun, F. Fan, J. Feng, Z. Wang, C. Z. Ning, *Nat. Nanotechnol.* **12**, 987–992 (2017).

[20] C. Ruppert, O. B. Aslan, T. F. Heinz, *Nano Lett.* **14**, 6231-6236 (2014).

[21] G. Froehlicher, E. Lorchat, S. Berciaud, *Phys. Rev. B* **94**, 085429 (2016).

[22] L. Zhou, K. Xu, A. Zubair, A. D. Liao, W. Fang, F. Ouyang, Y. H. Lee, K. Ueno, R. Saito, T. Palacios, J. Kong, M. S. Dresselhaus, *J. Am. Chem. Soc.* **137**, 11892-11895 (2015).

[23] T. A. Empante, Y. Zhou, V. Klee, A. E. Nguyen, I. H. Lu, M. D. Valentin, S. A. Naghibi Alvillar, E. Preciado, A. J. Berges, C. S. Merida, M. Gomez, S. Bobek, M. Isarraraz, E. J. Reed, L. Bartels, *ACS Nano* **11**, 900-905 (2017).

[24] I. G. Lezama, A. Arora, A. Ubaldini, C. Barreteau, E. Giannini, M. Potemski, A. F. Morpurgo, *Nano Lett.* **15**, 2336 (2015).

[25] A. Castellanos-Gomez, M. Buscema, R. Molenaar, V. Singh, L. Janssen, H. S. J. van der Zant, G. A. Steele, *2D Mater.* **1**, 011002 (2014).

[26] I. G. Lezama, A. Ubaldini, M. Longobardi, E. Giannini, C. Renner, A. B. Kuzmenko, A. F. Morpurgo, *2D Mater.* **1**, 021002 (2014).

[27] Y. Akahane, T. Asano, B. S. Song, S. Noda, *Opt. Express* **13**, 1202-1214 (2005).

[28] S. L. Portalupi, M. Galli, C. Reardon, T. F. Krauss, L. O'Faolain, L. C. Andreani, D. Gerace, *Opt. Express* **18**, 16064-16073 (2010).

[29] R. Lo Savio, S. L. Portalupi, D. Gerace, A. Shakoor, T. F. Krauss, L. O'Faolain, L. C. Andreani, M. Galli, *Appl. Phys. Lett.* **98**, 201106 (2011).

[30] D. Mao, B. Du, D. Yang, S. Zhang, Y. Wang, W. Zhang, X. She, H. Cheng, H. Zeng, J. Zhao, *Small* **12**, 1489-1497 (2016).[31] Z. Sun, T. Hasan, F. Torrisi, D. Popa, G. Privitera, F. Wang, F. Bonaccorso, D. M. Basko, A. C. Ferrari, Graphene mode-locked ultrafast laser. *ACS Nano* **4**, 803-810 (2010).

[32] Y. Yu, W. Xue, E. Semenova, K. Yvind, J. Mork, Demonstration of a self-pulsing photonic crystal Fano laser. *Nature Photonics* **11**, 81-84 (2016).

[33] A. Shakoor, R. Lo Savio, P. Cardile, S. L. Portalupi, D. Gerace, K. Welna, S. Boninelli, G. Franzò, F. Priolo, T. F. Krauss, M. Galli, L. O'Faolain, *Laser Photon. Rev.* **7**, 114-121 (2013).

[34] S. Matsuo, A. Shinya, T. Kakitsuka, K. Nozaki, T. Segawa, T. Sato, Y. Kawaguchi, M. Notomi, *Nat. Photon.* **4**, 648-654 (2010).

[35] H. Altug, J. Vučković, *Opt. Express* **13**, 8819-8828 (2005).

[36] Y. Q. Bie, G. Grosso, M. Heuck, M. M. Furchi, Y. Cao, J. Zheng, D. Bunandar, E. Navarro-Moratalla, L. Zhou, D. K. Efetov, T. Taniguchi, K. Watanabe, J. Kong, D. Englund, P. Jarillo-Herrero, *Nat. Nanotechnol.* **12**, 1124–1129 (2017).

[37] M. Amani, D. H. Lien, D. Kiriya, J. Xiao, A. Azcatl, J. Noh, S. R. Madhvapathy, R. Addou, K. C. Santosh, M. Dubey, K. Cho, R. M. Wallace, S. C. Lee, J. H. He, J. W. Ager, X. Zhang, E. Yablonovitch, A. Javey, *Science* **350**, 1065-1068 (2015).

[38] F. Withers, O. Del Pozo-Zamudio, A. Mishchenko, A. P. Rooney, A. Gholinia, K. Watanabe, T. Taniguchi, S. J. Haigh, A. K. Geim, A. I. Tartakovskii, K. S. Novoselov, *Nat. Mater.* **14**, 301-306 (2015).

Figures and Tables

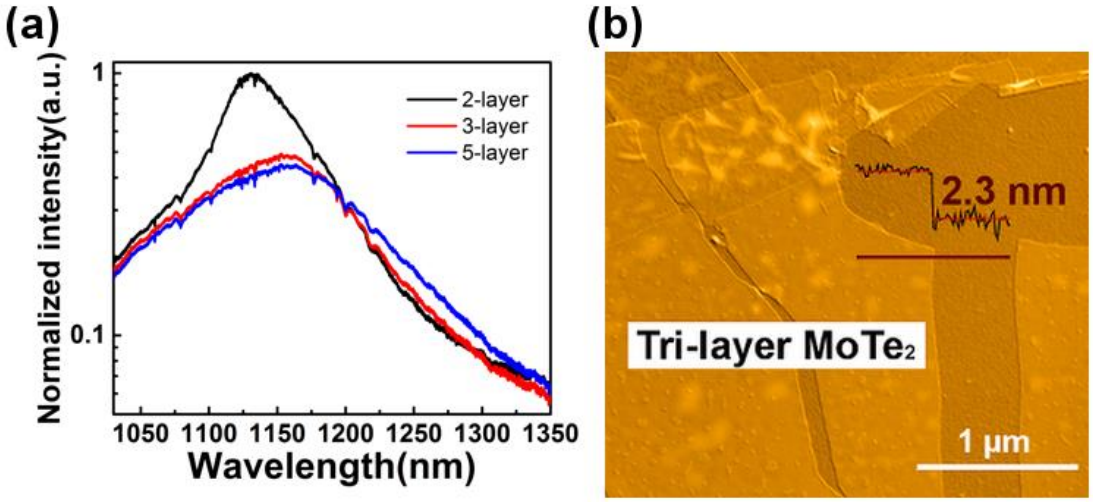

Figure 1. PL characterization. PL emission obtained at room temperature of bi-, tri- and penta (5)-layer $MoTe_2$ flakes. (**a**) PL spectra collected with a 785 nm CW excitation laser (1.68 mW excitation power and 1 μm spot size on the sample surface). (**b**) Corresponding atomic force microscope (AFM) profile showing the thickness of the tri-layer $MoTe_2$ flake exfoliated on a

silicon substrate. Since a monolayer is approximately 0.7 nm thick, 2.3 nm represents a trilayer.

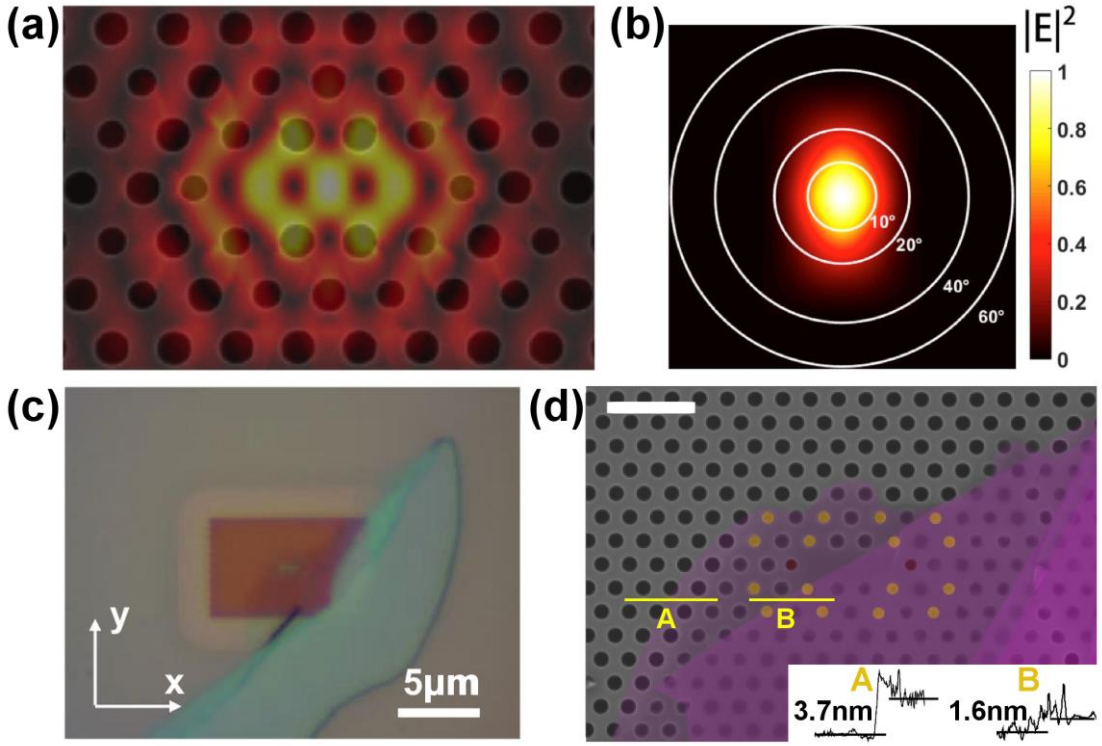

Figure 2. $MoTe_2$ on silicon photonic crystal cavity. Calculated electric field profile $|E|^2$ of a L3 PhC nanocavity for (**a**) the fundamental mode M1 and (**b**) its corresponding far-field emission. (**c**) Optical micrograph and (**d**) false-colored SEM image of a few-layer $MoTe_2$ flake on the silicon PhC cavity and corresponding AFM topography profiles; the scale bar in (d) represents 1 μm. We define the x and y directions in (c) to align with the ΓK and ΓM direction of the PhC cavity, respectively.

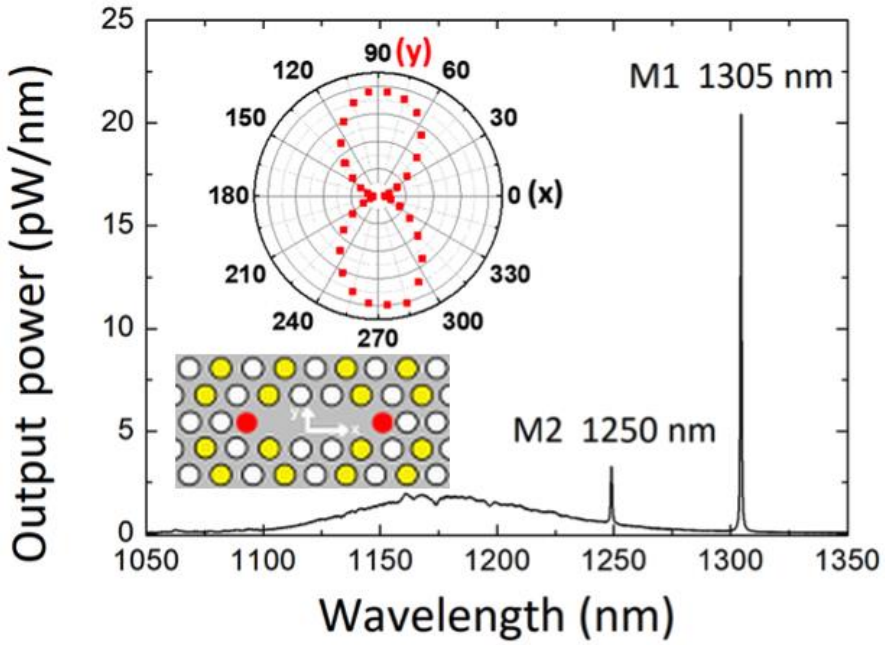

Figure 3. Dual-mode emission and polarisation. Emission spectrum of optically pumped $MoTe_2$-on-silicon laser at room temperature with a pump power of 1.9 mW; the fundamental mode (M1) is observed at 1305 nm and a higher order mode (M2) at 1250 nm. Inset: polarization characteristic of the M1 mode, with the x and y directions indicating the L3 cavity orientation, using the same coordinate system as in Figure 2.

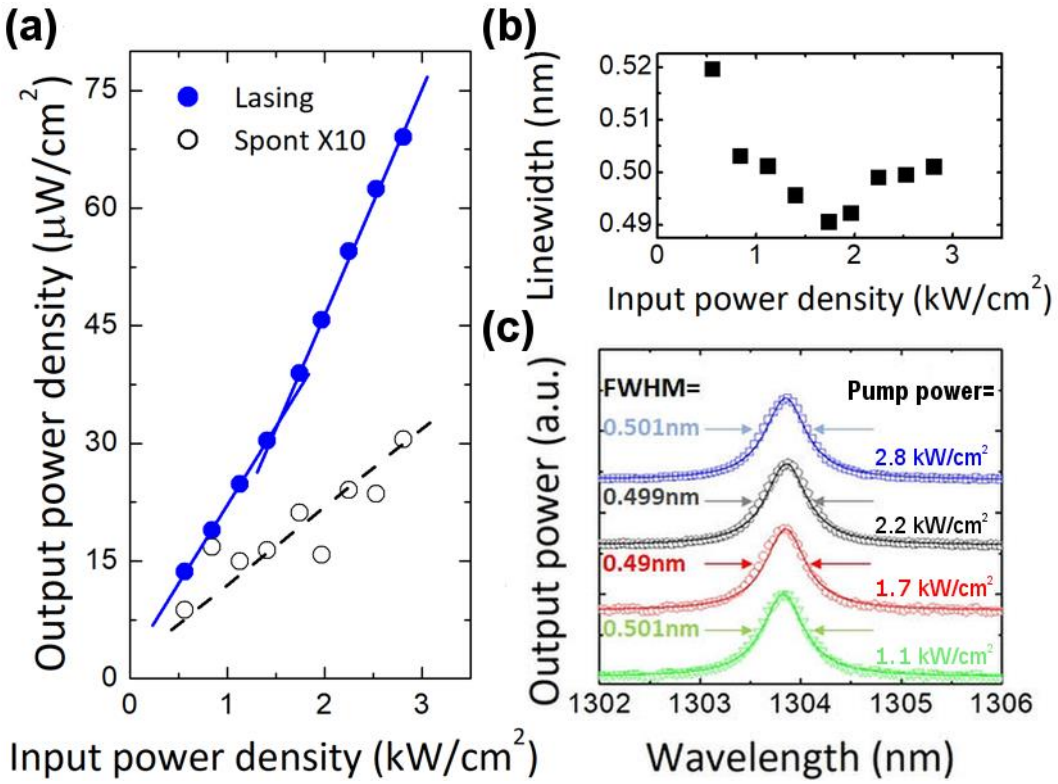

Figure 4. Laser threshold and linewidth. (**a**) The output power density of the fundamental laser mode (blue dots) and spontaneous emission (magnified by 10) at the same wavelength (black circles) as a function of pump power density incident on the sample surface. The fitted straight lines are guides to the eye. The kink in the laser emission indicates a lasing threshold of 1.5 kW/cm^2. (**b**) Linewidth of emission at 1305 nm as a function of the pump power. (**c**) Fundamental mode output spectra (dots) and the corresponding Lorentzian fits (solid curves) for different pump powers.

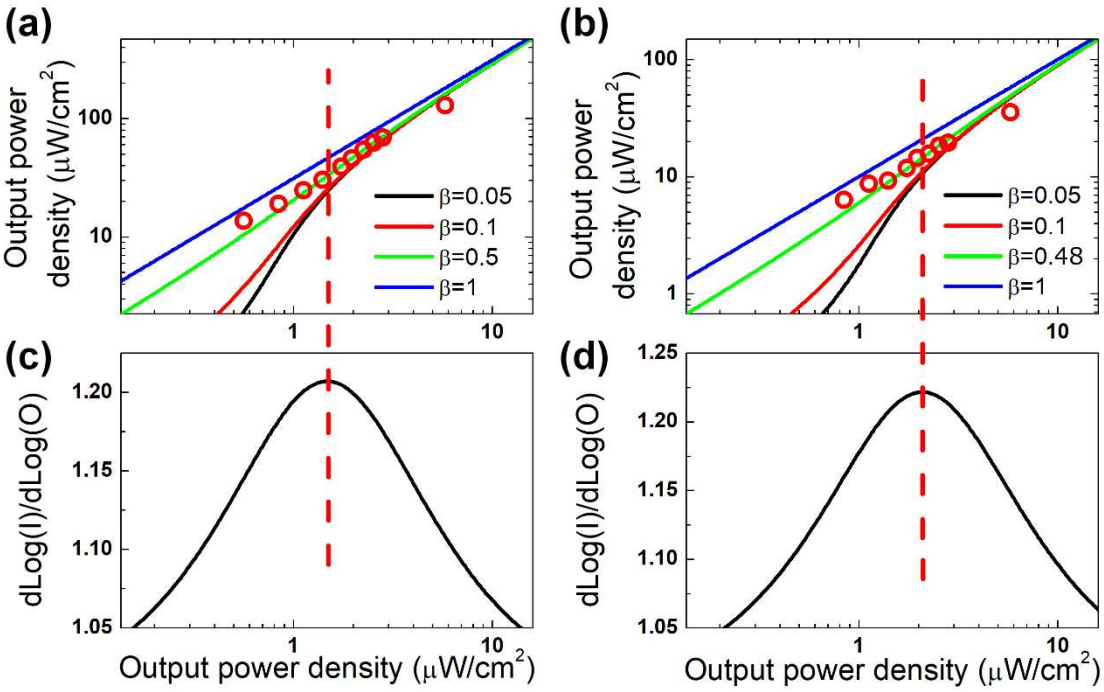

Figure 5. Laser threshold and β-factor. (**a**-**b**) Output power density as a function of the excitation power density of (**a**) the M1 and (**b**) the M2 mode. The red dots represent experimental data and the solid curve is a fit to the laser rate equation, corresponding to a spontaneous emission coupling factor $\beta = 0.5$ for M1 and $\beta = 0.48$ for M2. Calculated curves for other values of β are plotted for comparison. (**c**-**d**) First order derivative curve of the laser rate equation of M1 and M2 mode respectively - the vertical dashed lines (red) indicate the peak position, i.e. lasing thresholds (see SI).

Table 1. Performance comparison of various 2D material based lasers

Reference	Gain Material	Lasing Wavelength (nm)	Operating Temperature (K)	Pump Source	Hot cavity Q-factor[a)]	Threshold[b)] (W/cm^2)
[14]	WSe_2	740	130	CW	2,465	1
[15]	WS_2	612	10	Pulse	2,605	5-8 x 10^6
[16]	MoS_2	600-800	300	CW	~3,000	7140
[17]	$MoTe_2$	1132	300	CW	5,603	2100 [2c)]
This work	$MoTe_2$	1305	300	CW	2,660	1500

[a)]The "hot cavity" Q factor is derived from the lasing mode; [b)]We calculate the threshold from the total power incident on the sample surface and divide it by the pump spot area without taking any other effects such as power coupling into account; [c)]The threshold value in [17] is reported to be 6.6 W/cm^2. This quoted value is lower because the authors took absorption and coupling coefficients into account, which is not typically done by other authors.

Graphical Abstract

A few-layer 2D material (Figure 1) based 1305 nm silicon laser-like emission by putting $MoTe_2$ flakes onto L3-type photonic crystal cavities (Figure 2), operating in the center of the "O-band" used in optical communications under room temperature (Figure 3), and with a threshold power density as low as 1.5 kW/cm^2 (Figure 4 and Figure 5). The ability to use few-layer material enables the available production of large-area $MoTe_2$ flakes by manufacturing methods, such as chemical vapour deposition, which opens new opportunities for the on-chip optoelectronics integrated with multiple functional device, and thereby brings 2D-on-silicon devices a step closer to becoming a scalable technology.